

FFT-PCA Image Fusion Based Flora and Vegetation Mapping of Eshkevarat no Hunting Zone

**Zeinab Hoseinnejad^{*a}, Hasan Hasani Moghaddam^b, Zahra Parvar^c, Kouros Kavousi^d,
Hamid Gashtasb Meigooni^e**

^aM.Sc. Environmental Assessment, College of Environment, Department of Environment, Karaj, Iran

^bM.Sc. of Remote Sensing, Kharazmi University, Tehran, Iran

^cM.Sc. Environmental Assessment, Department of Environment, Faculty of Natural Resources, Malayer University, Iran

^dPh.D. Department of Biology, Science and Research Branch, Islamic Azad University, Tehran, Iran

^eAssociate Professor, Department of Natural Environment and Biodiversity, College of Environment, Karaj, Iran

Received 11 December 2019; revised 14 February 2020; accepted 10 March 2020

Abstract

The fusion of remote sensing data is essential in order to obtain more information from different images. Mapping the vegetation of an area is very important due to its environmental importance. In this research, Landsat ETM+ images and field surveying was used to identify vegetation states of the Eshkevarat no hunting zone. After applying necessary pre-processing like gap filling and atmospheric correction, the panchromatic and multi-spectral images were fused based on the FFT-PCA algorithm. In the next section the fused image was classified based on the Support Vector Machine (SVM), algorithm into five classes. The results showed that the overall accuracy and kappa coefficient of classified images is 0.943% and 0.910 respectively. In order to field surveying of study area, 1-meter plots in 500-meter distance choose and 14 Flora and vegetation species were identified and mapped. The results showed that satellite images have good accuracy in this field but based on its spatial resolution limitations a large number of species present in the area have not been identified. In this research, it is suggested to use a combination of both satellite image sources and field surveys.

Keywords: FFT-PCA, Flora and Vegetation, Landsat ETM⁺, SVM, Eshkevarat.

* Corresponding author: +98-9021423272.
Email address: zeinab.hoseinnejad@gmail.com

1. Introduction

Remote sensed data have been used to extract relevant information on various natural resources and environments (Zeaiean Firooz Abadi & Hasani Moghaddam, 2018). Image fusion is a sufficient way of retrieving information from multiple sources into one image (Hasani Moghaddam et al., 2019). With the emergency of a wide variety of remote sensing instruments and the widespread application of remote sensing data, multi-resolution images fusion is becoming increasingly more important (Song et al., 2014). In many research image fusions is used to achieve better results (De Juan et al., 2019). Vegetation analysis (Ghimire et al., 2020), mineral mapping (Contreras et al., 2019), Forest analysis (Tusa et al., 2019), and natural hazard monitoring (Belgiu and Stein., 2019), are as part of remotely sensed images fusion applications in environmental studies. Meanwhile, identifying the vegetation status of an area is considered as one of the most important indicators of environmental assessment. Flora is a collective term for a group of plant life found in a particular region (Tzankov et al., 2013).

Xie et al., (2008) investigated a review study in remote sensing imagery in vegetation mapping. This paper focuses on the comparisons of popular remote sensing sensors, commonly adopted image processing methods, and prevailing classification accuracy assessments. Important findings the basic concepts, available imagery sources, and classification techniques of remote sensing imagery related to vegetation mapping were introduced, analyzed, and compared. The advantages and limitations of using remote sensing imagery for vegetation cover mapping were provided to iterate the importance of a thorough understanding of the related concepts and careful design of the technical procedures, which can be utilized to study vegetation cover from remotely sensed images.

Gadal et al., (2019) analyzed urban vegetation mapping by use of satellite images. This study explored to what extent remote sensing imagery could be used to detect and to characterize urban vegetation. Two types of imagery were tested which are low-resolution satellite (i.e., Sentinel 2 and Landsat 8 OLI) and high-resolution airborne (i.e., Rikola hyperspectral sensor), the study assessed the detectability of vegetation species over Kaunas city (Lithuania) for different seasonal acquisitions. Satellite imagery showed accurate detection of 3 coarse classes of vegetation with overall accuracies (O.A.) superior to 90%, and airborne hyperspectral imagery showed decent detection of 13 fine classes of vegetation with O.A. of up to 73%.

Ghasemiane Sorboni et al., (2019) mapped vegetation by use of sentinel-1 and sentinel-2 images. The Sentinel-2 dataset is more suitable for vegetation mapping because a wide variety of vegetation indexes can be extracted from them. Handling this large number of vegetation indexes needs a robust feature extractor. Convolutional Neural Networks (CNN) extract relevant features through their deep feature layers structure and throw out disturbances from small to large scales. Hence, they can be far useful for classifying remote sensing data when the number of input bands is considerable. After pre-processed Sentinel-1 and 2 datasets and extracted the dual-polarized and optical vegetation indexes, the sentinel-1 vegetation indexes alongside the VV and VH sigma Nought bands to a Random Forest (RF) and 1D CNN classifier. Also, 13 spectral features of the Sentinel-2 and the extracted indexes like Blue Ratio (BR), Vegetation index based on Red Edge (VIRE), and Normalized Near Infrared (NNIR) were imported to an RF and 1D CNN. They classification result of Sentinel-1 data showed that Dual Polarized Soil Vegetation Index (DPSVI) is a good indicator for discriminating vegetation pixels. Also, the experiment on the Sentinel-2 dataset using 1D CNN resulted in True Positive Rate (TPR) and False Positive Rate of 0.839 and 0.034, respectively.

The aim of this study is to evaluate the vegetation cover of the Eshkevaart No hunting zone region using the fusion of Landsat ETM+ multispectral and panchromatic data. In this research, in addition to satellite analysis of the vegetation of the study area, mapping and field data collection have also been

used. Compared to similar research in this field (Afrin et al., 2019; Li et al., 2020), have used satellite imagery, In the present study, in addition to using satellite data processing, field mapping has been identified and prepared in the field.

2. Material and Methods

2.1 Study Area

The study area is called the "Eshkevarat No hunting zone" in Rudсар city, North of Iran. The area is 30347 ha and its environment is 82 km. Samamos Mountain with a height of 3670 meters is the highest mountain in the study area. Figure (1), Shows the location of the study area.

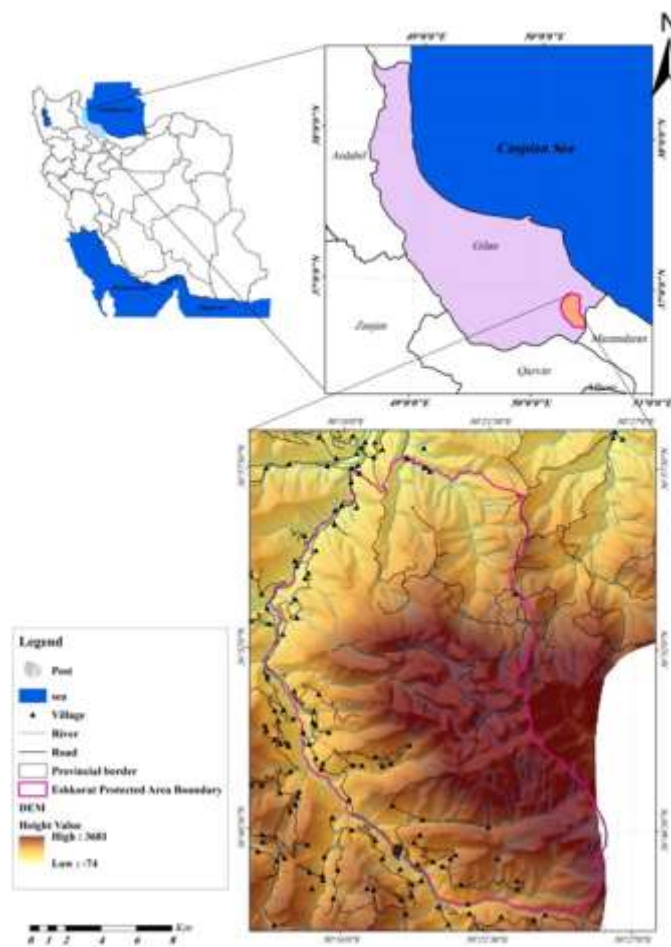


Figure 1. Location of the study area

2.2 Satellite Data Used

Landsat ETM+ provides 7-spectral bands (30_meter resolution) and a panchromatic band (15-meter resolution). Given that the study area was located on two images of the Landsat, two Landsat ETM+

166-35 and 166-34 path and row number images respectively acquired.

2.3 Image Pre-processing

On May 31, 2003, the Scan Line Corrector (SLC), which compensates for the forward motion of the satellite, was failed. Subsequent efforts to recover the SLC were not successful, and the failure is permanent. Without an operating SLC, the sensor’s line of sight traces a zig-zag pattern along the satellite ground track (Chen et al., 2011). Landsat ETM+ images filling the gap is the first preprocessing task that was done.

2.4 Methods

In order to improve the spatial resolution of Landsat ETM+ images, multispectral and panchromatic images of this sensor were fused using the FFT-PCA method. Due to the fact that this method has given acceptable results (Zeaiean Firooz Abadi and Hasani Moghaddam, 2018), this method has been used. After fusion of the images, a vegetation map, and field surveys were prepared. Image classification was performed using the SVM method.

2.5 Principal Component Analysis (PCA)

PCA is a common technique for dimensionality reduction (DR) and finding a pattern in high dimension data. Proposed by Pearson in 1901, it is based on the computation of low- dimensional representation of a high- dimensional dataset that maximizes the total scatter which is optimal in reconstruction. The following describes the description in steps (Zeaiean Firooz Abadi and Hasani Moghaddam, 2018):

Step1. The m samples can be represented by a set $\Psi = \{X_1, X_2, \dots, X_m\}$. For each sample, which has n indicators, it can be described as $\Psi = \{X_1, X_2, \dots, X_m\}$ for $i \in \{1, 2, \dots, m\}$, and then an $m \times n$ matrix X can be constructed with all the observation as follows:

$$X = \begin{bmatrix} X_1 \\ X_2 \\ \vdots \\ X_m \end{bmatrix} = \begin{bmatrix} X_{11} & X_{12} & \dots & X_{1n} \\ X_{21} & X_{22} & \dots & X_{2n} \\ \vdots & \vdots & \vdots & \vdots \\ X_{m1} & X_{m2} & \dots & X_{mn} \end{bmatrix} \tag{1}$$

Then based on Matrix X , the standardized matrix X^* can be obtained by the following procedure.

$$X^* = \begin{bmatrix} X_1^* \\ X_2^* \\ \vdots \\ X_m^* \end{bmatrix} = \begin{bmatrix} X_{11}^* & X_{12}^* & \dots & X_{1n}^* \\ X_{21}^* & X_{22}^* & \dots & X_{2n}^* \\ \vdots & \vdots & \vdots & \vdots \\ X_{m1}^* & X_{m2}^* & \dots & X_{mn}^* \end{bmatrix} \tag{2}$$

Where $X_i^* = (x_{i1}^*, x_{i2}^*, \dots, x_{in}^*)$, $x_{ij}^* = \frac{x_{ij} - \bar{x}_j}{\sqrt{\text{var}(x_j)}}$ is the value of the element in the

X^* after standardizing, $x_{ij} = (1/n) \sum_k = 1x_{ij}$ and $\text{var}(x_j) = (1/(n-1)) \sum_i = 1(x_{ij} - x_j)^2$ is the average value and the variance of the j^{th} column of X respectively, for $i \in \{1, 2, \dots, m\}$ and $j \in \{1, 2, \dots, n\}$.

Step 2. Then we can obtain the correlation matrix R based on the matrix X^* .

$$R = \begin{bmatrix} r_{11} & r_{12} & \dots & r_{1n} \\ r_{21} & r_{22} & \dots & r_{2n} \\ \vdots & \vdots & \vdots & \vdots \\ r_{m1} & r_{m2} & \dots & r_{mn} \end{bmatrix} \quad (3)$$

Where the value of the element r_{ij} in the matrix R can be calculated as follows:

$$r_{ij} = \frac{\sum_k = 1(x_{ki}^* - x_i^*)(x_{kj}^* - x_j^*)}{\sqrt{\sum_k = 1(x_{ki}^* - x_i^*)^2 \sum_k = 1(x_{kj}^* - x_j^*)^2}} \quad (4)$$

Where $x_i^* = (1/n) \sum_j = 1x_{ij}^*$, for $i \in \{1, 2, \dots, n\}$ and $j \in \{1, 2, \dots, m\}$.

Step 3. The n eigenvalues $\lambda_1 \geq \lambda_2 \geq \dots \geq \lambda_n > 0$ of matrix R and the corresponding n eigenvectors a_1, a_2, \dots, a_n can be obtained,

$$a_1 = \begin{bmatrix} a_{11} \\ a_{21} \\ \vdots \\ a_{n1} \end{bmatrix}, \quad a_2 = \begin{bmatrix} a_{12} \\ a_{22} \\ \vdots \\ a_{n2} \end{bmatrix}, \quad \dots, \quad a_n = \begin{bmatrix} a_{1n} \\ a_{2n} \\ \vdots \\ a_{nn} \end{bmatrix} \quad (5)$$

Then we can get n principal components as follows:

$$F_i = a_{1i} \times X_1^* + a_{2i} \times X_2^* + \dots + a_{ni} \times X_m^*, \quad (i = 1, 2, \dots, n). \quad (6)$$

Step 4. Compute the contribution rate CR_i and the accumulative contribution rate ACR_i of each principal component F_i ($i = 1, 2, \dots, n$), respectively:

$$CR_i = \frac{\lambda_i}{\sum_k = 1 \lambda_k},$$

$$ACR_i = \sum_{k=1}^i CR_k \quad (7)$$

Usually retain the top t principal components F_1, F_2, \dots, F_t , which correspond to the eigenvalues $\lambda_1, \lambda_2, \dots, \lambda_t$, and the corresponding accumulated contribution rate should satisfy that $ACR - t \geq 85\%$

Step 5. Through plugging the elements in the matrix X^* into the expression of t principal components, we can obtain the score matrix F .

$$F = \begin{bmatrix} F_{11} & F_{12} & \dots & F_{1t} \\ F_{21} & F_{22} & \dots & F_{2t} \\ \vdots & \vdots & \vdots & \vdots \\ F_{m1} & F_{m2} & \dots & F_{mt} \end{bmatrix} \tag{8}$$

Where $F_{ij} = a_{1j}x_{i1} + a_{2j}x_{i2} + \dots + a_{mj}x_{in}$ for $i \in \{1, 2, \dots, m\}$ and $j \in \{1, 2, \dots, t\}$.

Therefore, the original matrix X was transformed into matrix F that has reduced dimensionally, while not losing much information of the original data.

Step 6. The score matrix $F = [F_{ij}]_{m \times t}$ is a $m \times t$ matrix, can obtain the i^{th} samples total points (TP), $TP_i = \sum_{j=1}^t F_{ij} \times CR_j$, where CR_j is the j^{th} eigenvalues contribution rate.

2.6 Fast Fourier Transform

The Fast Fourier Transform (FFT), is used as a noise reduction mechanism during image processing. The FFT is a computationally efficient algorithm used to compute the Discrete Fourier Transform (DFT), and its inverse (IDFT). The FFT algorithm reduces the computational burden to $(N \log N)$ arithmetic operations. The FFT is a computationally efficient method of generating a Fourier transform (Zeaiean Firooz Abadi & Hasani Moghaddam., 2018).

The first stage in the execution of FFT during image processing is to compute the Discrete Fourier Transform. The DFT column vector, m_{jk} is represented mathematically as:

$$m_{jk}^* = DFT \{m_{jk}\} = \sum_{s=0}^{p-1} m_{jk} e^{-i(2\pi s j / p)} \tag{9}$$

Where $s = 0, 1, \dots, p - 1, j = 1, 2, \dots, n$ and $i = \sqrt{-1}$.

Where m_{jk} is the k^{th} column of the image matrix. For an image matrix of order $4, p = 4$ and $s = 0, 1, 2, 3$. The DFT becomes;

$$\begin{aligned} m_{j0k}^* &= m_{j0k} e^{-0.i\pi/2} + m_{j1k} e^{-0.i\pi/2} + m_{j2k} e^{-0.i\pi/2} + m_{j3k} e^{-0.i\pi/2}, \\ m_{j1k}^* &= m_{j0k} e^{-0.i\pi/2} + m_{j1k} e^{-1.i\pi/2} + m_{j2k} e^{-2.i\pi/2} + m_{j3k} e^{-3.i\pi/2}, \\ m_{j2k}^* &= m_{j0k} e^{-0.i\pi/2} + m_{j1k} e^{-2.i\pi/2} + m_{j2k} e^{-4.i\pi/2} + m_{j3k} e^{-6.i\pi/2}, \\ m_{j3k}^* &= m_{j0k} e^{-0.i\pi/2} + m_{j1k} e^{-3.i\pi/2} + m_{j2k} e^{-6.i\pi/2} + m_{j3k} e^{-9.i\pi/2}. \end{aligned} \tag{10}$$

Therefore,

$$\begin{bmatrix} m_{j0k}^* \\ m_{j1k}^* \\ m_{j2k}^* \\ m_{j3k}^* \end{bmatrix} = \begin{bmatrix} e^{-0.i\pi/2} & e^{-0.i\pi/2} & e^{-0.i\pi/2} & e^{-0.i\pi/2} \\ e^{-0.i\pi/2} & e^{-1.i\pi/2} & e^{-2.i\pi/2} & e^{-3.i\pi/2} \\ e^{-0.i\pi/2} & e^{-2.i\pi/2} & e^{-4.i\pi/2} & e^{-6.i\pi/2} \\ e^{-0.i\pi/2} & e^{-3.i\pi/2} & e^{-6.i\pi/2} & e^{-9.i\pi/2} \end{bmatrix} \begin{bmatrix} m_{j0k} \\ m_{j1k} \\ m_{j2k} \\ m_{j3k} \end{bmatrix} \quad (11)$$

And

$$\begin{bmatrix} m_{j0k}^* \\ m_{j1k}^* \\ m_{j2k}^* \\ m_{j3k}^* \end{bmatrix} = \begin{bmatrix} 1 & 1 & 1 & 1 \\ 1 & -i & -1 & i \\ 1 & -1 & 1 & -1 \\ 1 & i & -1 & -i \end{bmatrix} \begin{bmatrix} m_{j0k} \\ m_{j1k} \\ m_{j2k} \\ m_{j3k} \end{bmatrix} \quad (12)$$

The next stage is to compute the Inverse Discrete Fourier Transform (IDFT). The IDFT is given by:

$$m_{jk} = IDFT \{m_{jk}^*\} = \frac{1}{p} \sum_{r=0}^{p-1} m_{jk}^* e^{i(2\pi sr/p)}, \quad (13)$$

$s = 0, 1, \dots, p-1, j = 1, 2, \dots, n$ & $i = \sqrt{-1}$.

For $p = 4$ the IDFT is given by:

$$\begin{bmatrix} m_{j0k} \\ m_{j1k} \\ m_{j2k} \\ m_{j3k} \end{bmatrix} = \frac{1}{4} \begin{bmatrix} e^{-0.i\pi/2} & e^{-0.i\pi/2} & e^{-0.i\pi/2} & e^{-0.i\pi/2} \\ e^{-0.i\pi/2} & e^{-1.i\pi/2} & e^{-2.i\pi/2} & e^{-3.i\pi/2} \\ e^{-0.i\pi/2} & e^{-2.i\pi/2} & e^{-4.i\pi/2} & e^{-6.i\pi/2} \\ e^{-0.i\pi/2} & e^{-3.i\pi/2} & e^{-6.i\pi/2} & e^{-9.i\pi/2} \end{bmatrix} \begin{bmatrix} m_{j0k}^* \\ m_{j1k}^* \\ m_{j2k}^* \\ m_{j3k}^* \end{bmatrix} \quad (14)$$

And

$$\begin{bmatrix} m_{j0k} \\ m_{j1k} \\ m_{j2k} \\ m_{j3k} \end{bmatrix} = \frac{1}{4} \begin{bmatrix} 1 & 1 & 1 & 1 \\ 1 & i & -1 & -i \\ 1 & -1 & 1 & -1 \\ 1 & -i & 1 & i \end{bmatrix} \begin{bmatrix} m_{j0k}^* \\ m_{j1k}^* \\ m_{j2k}^* \\ m_{j3k}^* \end{bmatrix} \quad (15)$$

The method used in this research is very important due to the use of the integration of PCA and FFT algorithms in the image fusion process. Using this method, due to the advantages of each method alone,

causes better results. Given that most articles use traditional methods to image fusion, it can be said that the use of such a method is an innovation in this field.

2.7 Support Vector Machine (SVM)

A support vector machine is a useful technique for data classification (Abbasi et al., 2015). A classification task usually involves separating data into training and testing sets. Each instance in the training set contains one “target value” (i.e., the class labels) and several “attributes” (i.e., the features or observed variables). The goal of SVM is to produce a model (based on the training data) which predicts the target values of the test data given only the test data attributes (Hsu et al., 2003).

Given a training set of instance label point $(x_i, y_i), i = 1, \dots, l$ where $x_i \in R^n$ and $y \in \{1, -1\}^l$, the support vector machine (SVM) requires the solution of the following optimization problem:

$$\text{Min}_{w, b, \epsilon} \quad \frac{1}{2} w^T w + C \sum_{i=1}^l \epsilon_i$$

$$\text{Subject to} \quad y_i (w^T \phi(x_i) + b) \geq 1 - \epsilon_i, \quad \epsilon_i \geq 0. \quad (16)$$

Here training vectors x_i is mapped into a higher (maybe infinite) dimensional space by the function ϕ . SVM finds a linear separating hyperplane with the maximal margin in this higher-dimensional space. $C > 0$ is the penalty parameter of the error term. Furthermore, $K(x_i, x_j) = \phi(x_i)^T \phi(x_j)$ is called the kernel function. Though new kernels are being proposed by researchers, beginners may find in SVM books the following four basic kernels:

- Linear: $K(x_i, x_j) = x_i^T x_j$.
- Polynomial: $K(x_i, x_j) = (\gamma x_i^T x_j + r)^\alpha, \gamma > 0$.
- Radial Basis Function (RBF): $K(x_i, x_j) = \exp(-\gamma \|x_i - x_j\|^2), \gamma > 0$.
- Sigmoid: $K(x_i, x_j) = \tanh(\gamma x_i^T x_j + r)$.

Here, γ, r are kernel parameters.

3. Results and Discussion

Landsat ETM+ firstly corrected as gap_fill errors and then mosaicked. After performing the necessary preprocessing, the boundary of the study area was subsetted from the total images then panchromatic and multispectral bands of the images were fused with each other by the FFT-PCA method. Figure (2 & 3), shows the results of this processing.

Image fusion improved the spatial resolution of the images and made the selection of training data faster and more accurate in order to classify and identify the required areas. The FFT-PCA algorithm was used because of the superiority and acceptable results that were proven in the (Zeaiean Firooz Abadi and Hasani Moghaddam., 2018), and the results of evaluating the accuracy of this method show its high efficiency in image fusion. In fact, this method, by combining two PCA and Fast Fourier Transform algorithms and using the results of both, in addition to improving the quality of image fusion, also greatly reduces the image noises. Table (1), shows the results of the fusion accuracy assessment of the FFT-PCA method.

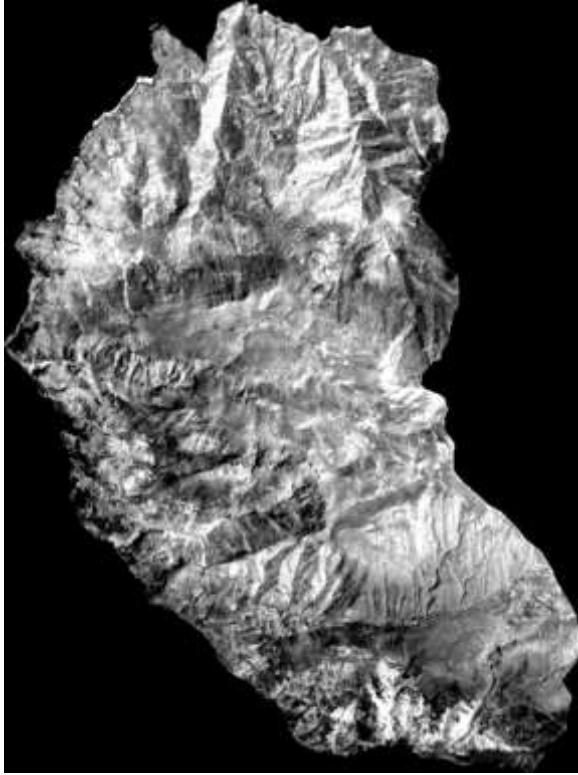


Figure 2. Study area masked from images

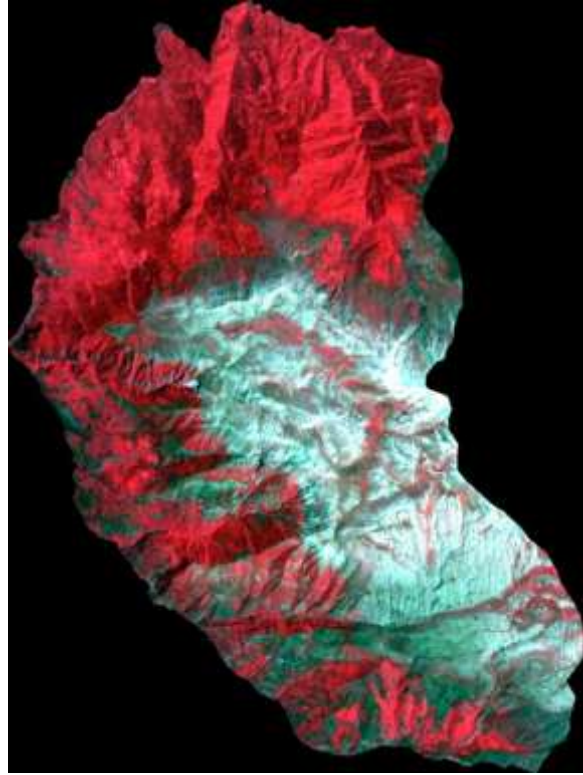


Figure 3. FFT-PCA fusion result

Table 1. Fusion result accuracy assessment

Accuracy assessment method	Result
DIV	0.0205
CC	0.974
Q	0.943
RMSE	1.010

The fused image was classified with five classes and by Support Vector Machine (SVM), algorithm. Forest land, sparse forest lands, rich rangelands, poor rangelands, and agricultural lands were extracted from the image. Accuracy assessment of image classification showed Kappa coefficient and overall accuracy 0.910 and 0.943 respectively. Figure (4), shows the SVM classification result.

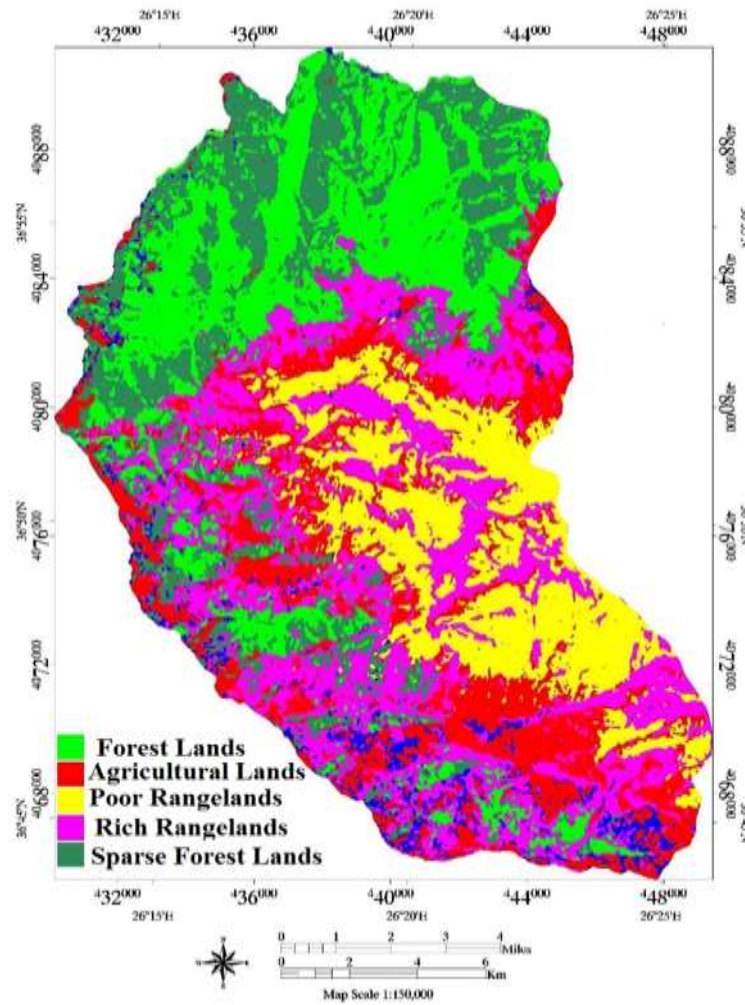


Figure 4. SVM classification result

In order to better identify the vegetation and flora of the area, the area was sampled in 1-meter plots at 500-meter intervals throughout the area. After identifying the vegetation, the vegetation map of the area was prepared based on the field activity. A total of 14 species were identified in these studies, the information of this species was shown in the Table (2).

Table 2. Vegetation and Flora species

Species code	Vegetation and Flora characteristic
IXU	No Vegetation

I	Thymus +Dactylis +Zozimia +(Crataegus) +Onobrychis + (Centaurea)
II	Carpinus +Zelkova + Cotoneaster + Crataegus + Lonicera
III	Carpinus + Parrotia +Zelkova + Alnus (sub)
IV	Carpinus + Crataegus + Pyrus + Berberis + Colutea + Lonicera
V	Berberis + Crataegus + Pyrus + Lonicera + Rosa
VI	Juniperus + Crataegus + Cotoneaster + Berberis + Astragalus
VII	Juniperus + Astragalus + Grasses
VIII	Carpinus + Zelkova + Alnus
IX	Onobrychis + Festuca + Astragalus
X	Fagus + Acer + Quercus + Carpinus + Fraxinus
XI	Carpinus + Quercus
XII	Carpinus + Zelkova +Mispilus
XIII	Cupressus sempervirens

The distribution map of the identified vegetation and flora species is given in the Figure (5).

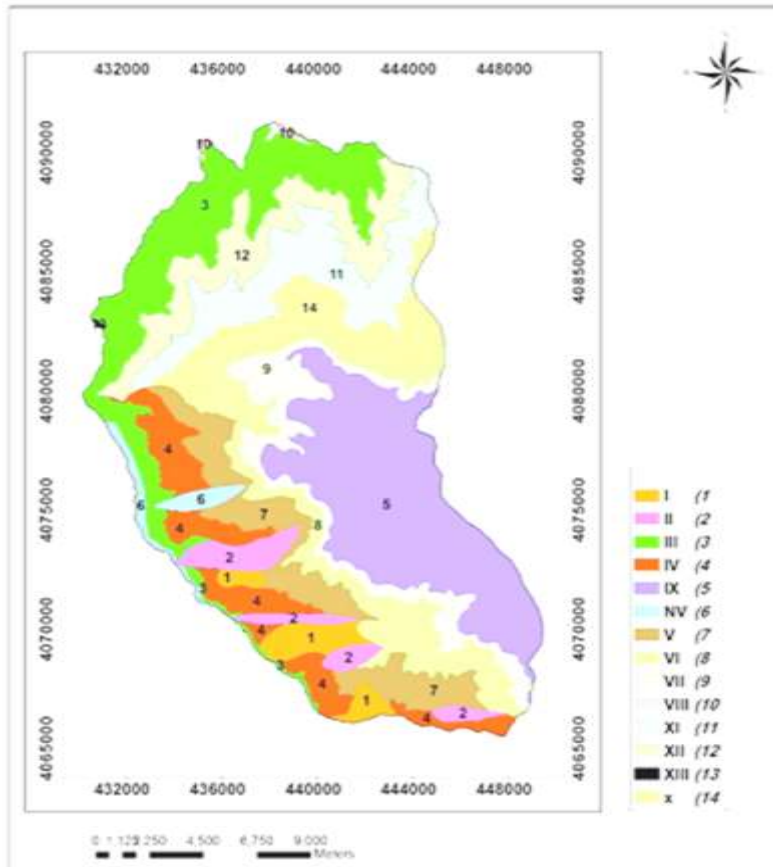


Figure 5. Vegetation and Flora map of field surveying

According to the results, satellite imagery is able to detect limited vegetation due to spatial resolution

limitations. Due to the fact that in the field evaluations the sampling rate was 1-meter plots, a lot of information was obtained. However, this type of assessment has drawbacks due to its time consuming and difficult access to the environment. In this research, the capability of both types of vegetation information extraction methods in the regions is presented, which can be used according to the needs of users. The results and findings of this research are consistent with (Ewald Fassnacht et al., 2019; Xie et al., 2019). In a comparison to (Hasani Moghaddam et al., 2019), in this paper, a hybrid method is used to image fusion. It can also be said that a newer method has been used compared to this article, which can prove the effectiveness of the use of hybrid methods in image fusion. In comparison to (Hasani Moghaddam and Torahi., 2018), who have used image fusion algorithms to investigate floods, in this research, a new fusion method has been used to study vegetation and flora.

4. Conclusion

Based on the results, it can be concluded that the simultaneous use of satellite images and field evaluations can lead to valuable results. Satellite images with higher spatial resolution can provide much better results than images with lower resolution. The use of methods to increase the spatial resolution of satellite images that are used in this research by the method of FFT-PCA can compete with field sampling, to provide more valuable results that due to limited access to high-resolution data, in this study It has a resolution of 15 meters. The results of this study showed that satellite images, despite the high speed of processing and obtaining information from them, have limited sampling compared to field methods. Although fieldwork is costly, a combination of both can be used with high-resolution data.

Reference

- Afrin, S., Gupta, A., Razu Ahmed, M., Achari, G., & Hassan, Q. (2019). Development of land use land cover maps using landsat-8 and MODIS data and their integration of Hydro ecological application. *Sensors*, 19.
- Abbasi, B., Arefi, H., Bigdeli, B., & Roessner, S. (2015). Automatic generation of training data for hyperspectral image classification using Support Vector Machine. *36th International Symposium on Remote Sensing of Environment, Berlin, Germany*.
- Belgiu, M., & Stein, A. (2019). Spatiotemporal image fusion in remote sensing. *Remote sensing*, 11, 1-20.
- Chen, J., Zhu, X., Vigelmann, J. E., Gao, F., & Jin, S. (2011). A simple and effective method for filling gaps in Landsat ETM+ SLC-off images. *Remote sensing of environments*, 115, 1053-1064.
- Contrerars, C., Khodadadzadeh, M., Tusa, L., Loidolt, Ch., Tolisana Delgado, R., & Gloaguen, R. (2019). *Geochemical and hyper spectral data fusion drill-core mineral mapping*. IEEE conference on Amsterdam, Netherlands, Netherlands.
- De June, A., Gowen, A., Duponchel, L., & Ruckebusch, C. (2019). Data handling in science and technology-Image fusion. *Science direct*, 31, 311-344.
- Ewald Fassnacht, F., Schiller, C., Kattenborn, T., Zhao, X., & Qu, J. (2019). A Landsat-based vegetation trend product of the Tibetan Plateau for the time-period 1990–2018. *Scientific data*, 78.
- Gadal, S., Ouerghemmi, W., Barlatier, R., & Mozferis, G. (2019). Critical analysis of urban vegetation mapping by satellite multispectral and airborne hyperspectral imagery. *5th International Conference on Geographical Information Systems Theory, Applications and Management. Greece*, (pp. 97-104)
- Ghasemiane Sorboni, N., Pahlavani, P., & Bigdeli, B. (2019). Vegetation mapping of sentinel-1 and sentinel-2 satellite images using convolutional neural network and random forest with the aid of dual polarized and optical vegetation indexes. *The International Archives of the Photogrammetry, Remote*

- Sensing and Spatial Information Sciences*, 42, 435-440.
- Ghimire, P., Lei, D., & Juan, N. (2020). Effect of image fusion on vegetation index quality –A comparative study from Gaofen-1, Gaofen-2, Gaofen-4, Landsat-8 OLI and MODIS imagery. *Remote sensing*, 12(10), 1550.
- Hasani Moghaddam, H., & Torahi, A. A. (2018). Determination of flood extent using OLI data (case study: Dezful 2016 flood). *Environment and Water Engineering*, 5(1), 24-35.
- Hsu, C. W., Chang, C. C., & Lin, C. J. (2003). A practical guide to support vector classification. 1396-1400.
- Hasani Moghaddam, H., Torahi, A. A., & Zeaiean Firooz Abadi, P. (2019). Using discrete wavelet transform to increase the accuracy of hyper spectral and high resolution images fusion. *Journal of Radar and Optic remote sensing*, 1, 22-30.
- Li, J., Li, A., He, L., Chen, J., & Plaza, A. (2020). Spatio-temporal fusion for remote sensing data: an overview and new benchmark. *Science China Information Sciences*, 63(4), 1-17.
- Song, H., Huang, B., Liu, Q., & Zhang, K. (2014). Improving the spatial resolution of Landsat TM/ETM+ through fusion with spot-5 images via learning-based super-resolution. *IEEE TRANSACTIONS ON GEOSCIENCE AND REMOTE SENSING*, 53(3), 1195-1204.
- Tusa, E., Laybros, A., Barre, J. B., Monnet, J., Dalla Murra, M., Dalponte, M., Vincent, G., Chanussot, J., & Berger, F.(2019). *Geophysical research abstract*, 21.
- Tzankov, N., Kunev, G., Grozdanov, A., & Parvanov, D. (2013). Analysis and data collection (flora and fauna) of the cross-border Maleshevska Mountain. In Conference: *IPA Cross-border programme, CCI No. 2007CB16IPO007, Full Report, Sofia, Bulgaria*.
- Xie, S., Liu, L., Zhand, X., Yang, J., Chen, X., & Gao, Y. (2019). Automatic Land-Cover Mapping using Landsat Time-Series Data based on Google Earth Engine. *Remote sensing*, 11(24), 3023.
- Xie, Y., Yu, M., & Sha, Z. (2008). Remote sensing imagery in vegetation mapping: A review. *Journal of planet ecology*, 1(1), 9-23.
- Zeaiean Firooz Abadi, P., & Hasani Moghaddam, H. (2018). Performance evaluation of FFT-PCA method based on dimensionality reduction algorithms in improving classification accuracy of OLI data. *Journal of Radar and Optic remote sensing*, 1(2), 24-37.